Hybrid PDE-ABM models: from oncology to virology

Abstract of Ph.D. Thesis

Sadegh Marzban

Supervisor:

Gergely Röst, associate professor, Ph.D.

Doctoral School of Mathematics
and Computer Science
University of Szeged, Bolyai Institute

Szeged

2023

Introduction

Mathematical models describing natural phenomena can be encoded into computer programs, and then the behaviour of the system can be simulated. Beyond representing equations defined in the mathematical models, computer simulations can offer higher flexibility and finer resolution than we can analyse by equation based models. In this work, we strive for taking advantages of both methods: combining differential equations with computational simulations, we have access to the insights gained from mathematical analysis, and also to the rich dynamical behaviours we can observe by performing a large amount of computations. A simulation utilizing agent-based modeling (ABM) involves capturing the properties and behaviors of abstract entities known as agents. Each agent in an ABM possesses characteristics and behaviors, and can act autonomously based on the environment and other agents in the model. This is similar to the concept of classes in many Object-Oriented languages. The interactions among agents in many ABMs lead to emergent behaviors that can only be described at the system level. An example can be found in the flocking of birds in which the birds exhibit properties similar to those of self-governing organisms. As emergent behavior is difficult to study directly, in contrast to the individual behavior of a single agent, ABMs are well suited to analyzing these types of complex systems. In this method, the fundamental idea is the definition of a discrete heterogeneous state space in which the elements or agents have collective interactions with each other and change their states accordingly [1]. This thesis utilizes ABM to investigate two biological phenomena. A model is developed to simulate the emergence of resistant cancer cells as a result of chemotherapy. We also study viral dynamics at the cellular level.

Development of resistance to chemotherapy in cancer patients strongly effects the outcome of the treatment. Due to chemotherapeutic agents, resistance can emerge by Darwinian evolution. Besides this, acquired drug resistance may arise via changes in gene expression. A recent discovery in cancer research uncovered a third possibility, indicating that this phenotype conversion can occur through the transfer of microvesicles from resistant to sensitive cells, a mechanism resembling the spread of an infectious agent. We present a model describing the evolution of sensitive and resistant tumour cells considering Darwinian selection, Lamarckian induction and microvesicle transfer.

We also establish an agent based model as a spatial version of the ODE model and compare the outputs of the two models. We find that although the ODE model does not provide spatial information about the structure of the tumour, it is capable to determine the outcome in terms of tumour size and distribution of cell types.

The results of our models demonstrate the recent observation that some cancer cells can be transferred by microvesicles. It would be natural to observe how microvesicles affect treatment along with other factors contributing to the spread of cancer cells.

We propose a hybrid partial differential equation – agent-based (PDE–ABM) model to describe the spatio-temporal viral dynamics in a cell population. The virus concentration is considered as a continuous variable and virus movement is modelled by diffusion, while changes in the states of cells (i.e. healthy, infected, dead) are represented by a stochastic agent-based model. The two subsystems are intertwined: the probability of an agent getting infected in the ABM depends on the local viral concentration, and the source term of viral production in the PDE is determined by the cells that are infected.

We develop a computational tool that allows us to study the hybrid system and the generated spatial patterns in detail. We systematically compare the outputs with a classical ODE system of viral dynamics, and find that the ODE model is a good approximation only if the diffusion coefficient is large.

We demonstrate that the model is able to predict SARS–CoV–2 infection dynamics, and replicate the output of *in vitro* experiments. Applying the model to influenza as well, we can gain insight into why the outcomes of these two infections are different.

We rigorously verify an experimental observation suggested by our previous simulations: once established, infections almost never disappear spontaneously. Using the powerful toolbox of branching processes we theoretically calculate the probability of extinction for a single cell and obtain an $\mathcal{O}(0.01)$ value corresponding to our expectations.

We also explore fundamental statistical features such as mean and a 95% confidence interval for the number of infected cells. The latter results visually confirm a satisfactory level of variability within the system: on the one hand it supports small and natural changes from outcome to outcome, on the other hand it clearly allows successful large-scale prediction and analysis as most infection curves remain close to the average.

We also investigate Paxlovid as a promising, orally bioavailable novel drug for SARS-CoV-2 with excellent safety profiles. Our main goal here is to explore the pharmacometric features of this new antiviral. To provide a detailed assessment of Paxlovid, we propose a hybrid multiscale mathematical approach. We demonstrate that the results of the present in silico evaluation match the clinical expectations remarkably well: on the one hand, our computations successfully replicate the outcome of an actual in vitro experiment; on the other hand, we verify both the sufficiency and the necessity of Paxlovid's two main components (nirmatrelvir and ritonavir) for a simplified in vivo case. Moreover, in the simulated context of our computational framework, we visualize the importance of early interventions and identify the time window where a unit-length delay causes the highest level of tissue damage. Finally, the results' sensitivity to the diffusion coefficient of the virus is explored in detail.
The dissertation is based on three articles of the author. These publications are the following:

[1] Attila Dénes, **Sadegh Marzban**, and Gergely Röst. Global analysis of a cancer model with drug resistance due to Lamarckian induction and microvesicle transfer. *Journal of Theoretical Biology*, 527, 110812, year = 2021 .

[2] **Sadegh Marzban**, Renji Han, Nóra Juhász, and Gergely Röst. A hybrid PDE-ABM model for viral dynamics with application to SARS-CoV-2 and influenza. *Royal Society Open Science*, 8(11), 210787, year = 2021 .

[3] Ferenc A. Bartha, Nóra Juhász, **Sadegh Marzban**, Renji Han, and Gergely Röst. In Silico Evaluation of Paxlovid's Pharmacometrics for SARS-CoV-2: A Multiscale Approach. *Viruses*, 14(5), 1103, year = 2022 .

Cancer

We established a mathematical model describing the evolution of tumour cells sensitive or resistant to chemotherapy. In the model, we considered three ways of emergence of chemotherapy resistance as a result of the therapeutic drug: Darwinian selection, Lamarckian induction and, based on recent discoveries, the emergence of resistance via the transfer of microvesicles from resistant to sensitive cells, which happens in a similar way as the spread of an infectious agent.

$$\begin{aligned} S'(t) &= -\beta S(t)R(t) - \theta S(t) + \rho_0 S(t)(K - S(t) - R(t)) - \mu_0 S(t) - pS(t), \\ R'(t) &= \beta S(t)R(t) + \rho_r R(t)(K - S(t) - R(t)) - \mu_r R(t) + pS(t). \end{aligned} \tag{1}$$

Our simple ODE model (1) certainly has its limitations. As we use ordinary differential equations, our model cannot provide information about the spatial structure of a tumour. To assess the capabilities of our model in describing tumour growth, we have also established a spatial version of the model in the form of an agent based model. In order to simulate the spatial model regarding to equation (1), we begin by defining the assumptions of the model and then describe the important technical aspects of the model in the implementation part. The following assumptions are considered for the ABM model.

1. There are two possible states for agents: we have sensitive or resistant cells.

2. If there is an empty space in the 8 cells Moore neighbourhood of each cell, both sensitive and resistant cells divide with a probability of birth, P_b, which is equal to P_S or P_R, depending on the type of the given cell.

3. Sensitive cells die due to apoptosis with rate μ_S, and due to drug effect with rate θ_{ABM}. Resistant cells die due to apoptosis with rate μ_R. Let P_d denote the probability of death. Hence, in sensitive cells $P_d = \mu_S + \theta_{ABM}$ and in resistant cells $P_d = \mu_R$.

4. Phenotype conversion from sensitive to resistant cells can happen due to Lamarckian induction, the rate of which we denote by P_{ABM}. Another way of phenotype conversion is due to the transfer of microvesicles between cells. This phenomenon is described by two parameters, namely the distance from resistant cells (if there exists resistant cell(s) in the von Neumann neighbourhood of each sensitive cell) and the rate of phenotype conversion due to microvesicles is denoted by β_{ABM} in this model.

Comparing the two models, we can deduce that the ODE model performs well in reproducing the possible outcomes of the tumour growth: as for total mass of the two cell types, there is no further scenario provided by the ABM than the ones experienced with the ODE model. Of course, this model will only give us information about the tumour mass and not about the spatial distribution of the two types of the tumour cells or the direction of spatial growth of the tumour as it is shown in Figure 1. Also, the simulations suggest that the ODE model and the agent based model react in a similar way to parameter changes. Furthermore, the ODE model cannot describe the transfer of microvesicles as a spatial phenomenon in a way the ABM is capable to do so, although by modifying the parameter β in the ODE, in some extent we also consider the effect of distance between cells on the transfer of microvesicles.

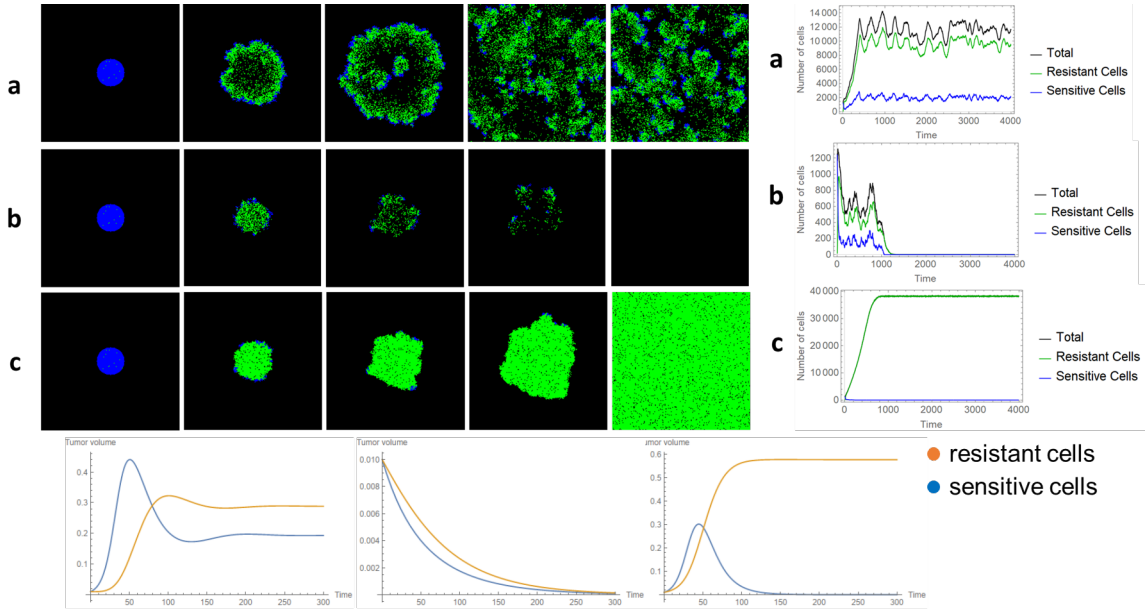

Figure 1: Possible outcomes with respect to drug concentration and the fitness of the resistant cells: partial response to therapy (a), tumour eradication (b), or treatment failure (c). Above is ABM outcome and below is ODE result.

In its present form, the effect of microvesicles and Lamarckian induction is described in a simple way in our model, especially in the simplified form (1). To consider these phenomena in a more realistic way can be subject of future research.

Viral dynamics for SARS-COV-2 and influenza

We have applied two different models for investigating the dynamical aspects of virus spread. The first model we considered was a hybrid PDE-ABM system (2), which is essentially a result of merging a discrete state space representing epithelial cells with a continuous reaction-diffusion equation grasping virus concentration.

$$\frac{\partial V^h(t,x,y)}{\partial t} = D_V \Delta V^h - \mu_V \cdot V^h(t,x,y) + \sum_{(i,j)\in\mathcal{J}} g_{i,j}(t,x,y), \quad t>0,\ (x,y)\in\Omega, \tag{2}$$

At the same time, we have used the so-called May-Nowak system – a well-known version of the classical ODE model (3) – as a reference system. As for theoretical completeness, we provide a rigorous analysis of both models in the Appendix, including a well-posedness result related to the hybrid model and the study of the ODE model's temporal dynamics.

$$\begin{cases} \frac{dH(t)}{dt} = -\beta H(t)V(t), & t>0, \\ \frac{dI(t)}{dt} = \beta H(t)V(t) - \delta I(t), & t>0, \\ \frac{dV(t)}{dt} = pI(t) - cV(t), & t>0, \\ \frac{dD(t)}{dt} = \delta I(t), & t>0, \\ H(0)=H_0\geq 0, I(0)=I_0\geq 0, V(0)=V_0\geq 0, D(0)=D_0\geq 0, \end{cases} \tag{3}$$

The hybrid model's computational implementation and the careful exploration of its results is in some sense the heart of our work – we highlight that our program code is based on a free and open source Java library, HAL (Hybrid Automata Library) [3], commonly used for oncology modeling.

The connection between the ODE model and hybrid PDE-ABM system

In this subsection we examine the relationship between the two main models' respective parameters. Expressing these connections is not always a trivial task as the hybrid PDE-ABM framework exists in space, while the ODE model's functions are defined as variables only in time. In order to match the two different systems' corresponding parameters, we need to fix some basic features of the spatial domain: first of all, let A denote the complete area of the state space; moreover, for simplicity let us assume that each cell has the area of a unit space – for the latter we introduce the notation σ^2. Finally, let τ denote the unit step in time.

1. **Parameters related to cell death:** We emphasise that the two main models use different approaches to quantify the chance of an infected cell's death – on the one hand, the (3) ODE model works with a δ death *rate*; on the other hand, the hybrid system uses a P_D *probability*. We can easily obtain a conversion between probability and rate by following the exact meaning behind these parameters. When infected cells die with a death rate δ, their natural decay can be described by the function $e^{-\delta t}$; hence, the probability of an infected cell's death between any two arbitrary time points t_1 and t_2 is given by

$$\frac{e^{-\delta t_1} - e^{-\delta t_2}}{e^{-\delta t_1}} = 1 - e^{-\delta(t_2 - t_1)}.$$

   Specifically, for a time interval of length τ the above formula means that an infected cell dies within that given time frame with a probability of $1 - e^{-\delta\tau}$.

   Applying the Taylor expansion of the exponential function and combining it with the fact that τ is small, we arrive to the $1 - e^{-\delta\tau} \approx \delta\tau$ approximation, i.e. we the connection between δ and P_D is given by

$$P_D \approx \delta \cdot \tau. \tag{4}$$

2. **Parameters related to new infections:** In this part we establish a connection between the ODE model's infection rate β and the hybrid system's probability of infection P_I. Similarly to the previous point, we need to quantify a relationship between parameters of different dimensions – one being a *rate*, the other a *probability* – but this time the solution is a bit more complex due to the role of spatial factors. We first focus on the hybrid model's P_I parameter solely within the context of the PDE-ABM system. We define the probability of a cell's infection in a way that this probability is

directly proportional to the local virus concentration $V^h(\Omega_{i,j})$ in the (i,j)-th cell (n.b. the number of viruses per unit space) and to the τ time unit, i.e. we have

$$P_I(V^h(\Omega_{i,j}), \tau) = \iota \cdot V^h(\Omega_{i,j}) \cdot \tau, \tag{5}$$

where ι is some appropriately set constant value. Our next step is to express the relationship between β and P_I for a specifically chosen, simplified scenario – we temporarily assume a homogeneous virus distribution over the domain Ω. Now, the key to expressing P_I in terms of β consists in carefully counting the newly infected cells over one iteration in both the ODE and the hybrid systems. Assuming H healthy cells and a V total number of viruses at a given time, the corresponding number in the ODE model is naturally $\beta \cdot V \cdot H \cdot \tau$. When we switch to the context of the spatial hybrid model, we need to keep in mind that the virus particles are now spread throughout the entire domain Ω, and as a consequence, a single cell is exposed only to the locally, physically present virus particles, whose number is $\bar{v} = V/A$. This means that the expected value of the total number of newly infected cells in the hybrid system is $H \cdot P_I(\bar{v}, \tau)$. Setting the respective values in the two main models equal leads us to

$$P_I(\bar{v}, \tau) = \beta \cdot A \cdot \bar{v} \cdot \tau. \tag{6}$$

The final step is to combine (5) and (6) – by substituting $V^h(\Omega_{i,j}) = \bar{v}$ in the former we immediately obtain $\iota = \beta \cdot A$. The connection between β and P_I is thus captured by

$$P_I(V^h(\Omega_{i,j}), \tau) = \beta \cdot A \cdot V^h(\Omega_{i,j}) \cdot \tau. \tag{7}$$

We highlight that the hybrid model's P_I parameter takes the above form exclusively when the PDE-ABM model's parameters are configured with a very specific goal in mind: to match the ODE system. Otherwise, when the hybrid software is used completely as a standalone, ι is simply a parameter in the hybrid model.

3. **Parameters related to virus production:** The (3) ODE model's parameter p corresponds to virus production rate per unit time. Respectively, in our spatial hybrid model's virus dynamical equation (2) the parameter $g_{i,j}$ represents the virus production rate per unit time per unit space[2] – in particular, $g_{i,j} = f_{i,j}$ within infected cells (see **??**), hence, clearly, $f_{i,j}$ matches p.

4. **Parameters related to virus removal:** Analogously, the respective pair of the hybrid model's m_V parameter is the ODE system's c virus removal constant.

5. **Parameters related to virus diffusion:** We highlight that the hybrid model's diffusive constant D_V does not have a corresponding parameter in the ODE system, as the latter model is defined only in time and diffusivity is strictly related to spacial dimensions.

Compared to the ODE system, both the decisive advantages and the main difficulties of the hybrid model are naturally related to the PDE-ABM system's added (and quite high-level) complexity: the inclusion of spatial effects. On the one hand, the limiting factors of this model include an increased computational demand and the fact that it is virtually impossible to consider a really large number of cells on an ordinary computer (we worked with a slice of tissue consisting of $4 \cdot 10^4$ cells). On the other hand however, this hybrid model provides us with the invaluable spatial distribution of infection spread: by running simulations for influenza and SARS-CoV-2 propagation, the results of our spatiotemporal PDE-ABM system suggested that influenza seems to generate sharper frontlines in virus concentration than COVID-19 does; moreover, especially for higher diffusion values, COVID-19 visibly spreads in a more homogeneous manner compared to influenza. This simply would not have been possible using the ODE model as the latter is defined only in time. The ODE system represents a scenario where all cells can interact with all virus particles, or in other words, it implicitly assumes an infinite diffusion coefficient in some sense. Real-life viruses however clearly have a finite diffusion rate. This also means that if the specific virus in question has a relatively low diffusion rate, then the ODE model's predictions regarding infection dynamics will be less accurate: the lower the diffusion coefficient, the more important it is to apply the more complex and more suitable spatial hybrid model.

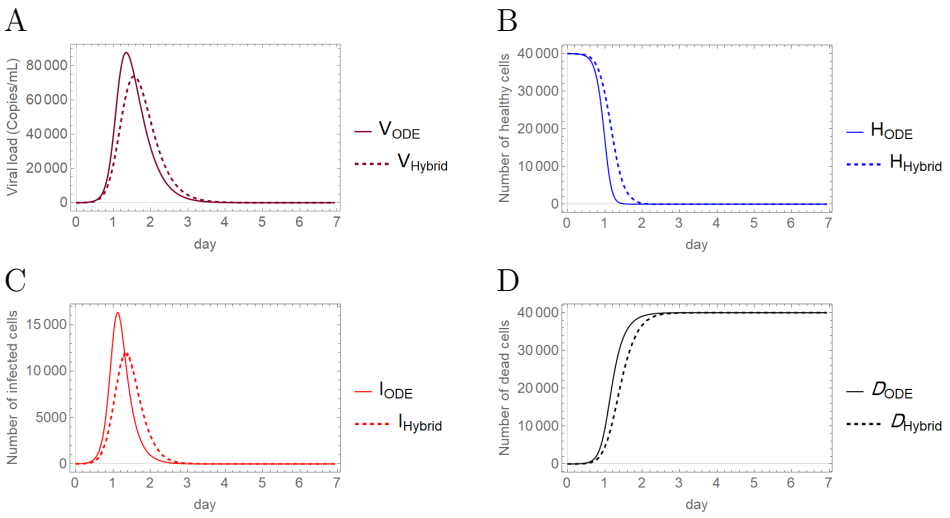

Figure 2: Comparison of the ODE model (solid lines) and the hybrid PDE-ABM model (dashed lines) for *influenza*. All figures depict a change taking place over the course of seven days; specifically, **A** Viral load (*copies/ml*), **B** Number of healthy cells, **C** Number of infected cells, **D** Number of dead cells.

In terms of verifying the accuracy and correctness of our proposed model, we have relatively successfully recreated the real results of a scientific *in vitro* experiment: our computer-simulated results matched the actual events and features of infection spread on a satisfactory level (Figure 3). Regarding correctness, we refer to Figure 2 as well: about 30 to 50% of the epithelial cells are destroyed in the upper respiratory system at the peak of infection, which corresponds to the observations of [4] and [5].

As for possible further improvements and applications of our hybrid spatial model, we

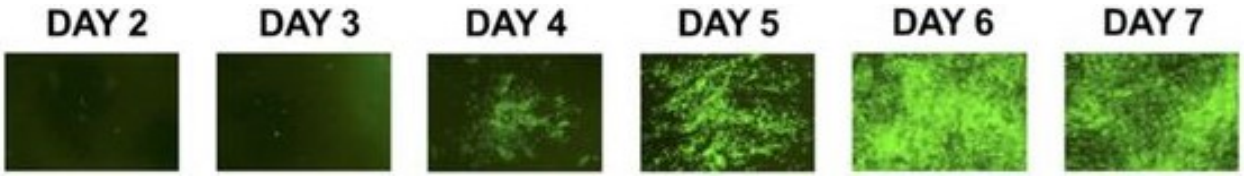

Experimental *in vitro* results of [10] assessing viral spread.

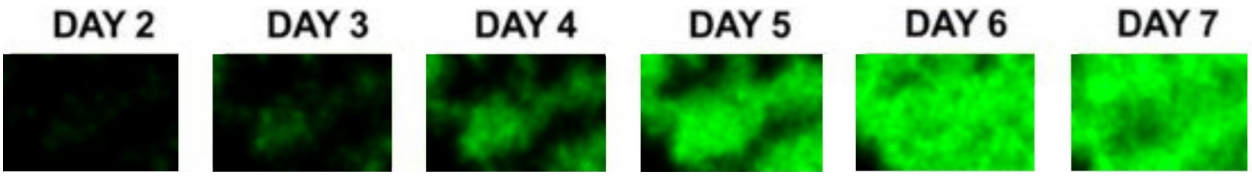

Figure 3: The simulated spatiotemporal dynamics of SARS–CoV–2 virus spread in human airway epithelial cells – the results were obtained by our source code implementing the hybrid PDE–ABM model. This sequence of pictures from our model output shows a striking resemblance to Figure(4B) in [10] (seen below), where the latter depicts real experimental results assessing viral propagation. *Note the colour choice we apply in this figure: in order to match our simulation's colours to the experimental results in [10], in this particular image the colour green represents virus particles and not healthy cells.*

mention two main points. Firstly; fine-tuning features such as immune response processes, time delay between infection and virus production, and the phenomenon of cell regeneration are ignored in our current study. These can be the subject of possible future work, although we note that the present model itself can also be considered to be highly realistic in specific cases where some of the above mentioned elements are naturally negligible (e.g. at the short early phase of an infection the immune system has typically not responded yet, while the time frame is too short for cell regeneration to be relevant). Secondly, we plan to apply the hybrid system for parameter fitting analogously as [4] used the ODE model for a similar task for the case of influenza A. In more detail, the authors of [4] calculated a best fit of the ODE model using experimental data on viral load – they extracted viral kinetic parameters such as infection rate, virus production rate, viral clearance rate, and the half-life of free infectious viruses. We simulated the corresponding scenario with both systems and – as expected, considering the relatively low diffusion value set for influenza – there was an apparent difference between the respective numerical solutions of the ODE model and the hybrid system. According to our results, [4] somewhat underestimates the R_0 value: as Figure 2 shows, in order to obtain a solution with the PDE-ABM model that corresponds to the ODE solution (and hence, to the real curve), it seems that the R_0 value of the hybrid model needs to be higher than the value estimated by [4] to fit the experimental data. This is another example of how the assumption of homogeneous virus spread can be misleading – the kinetic values obtained by [4] could be adjusted towards their real biological value by means of the hybrid PDE-ABM model. Thus, parameter estimation and fitting the stochastic hybrid model to various virological data is something we also consider as valuable future work.

The complex hybrid approach allows our model to capture fundamental physical processes such as diffusion. We have seen that this is paramount in analysing spatiotemporal virus

spread, but we emphasise that virus diffusion itself is not the only example for this feature's significance. Future works using this framework may consider immune response or antiviral drugs. For the latter, drug diffusion is essential, since spatial heterogeneity naturally arises as the drug enters the tissue through the capillary network. Hence, the diffusive property has a key role in the analysis of antiviral drug effectiveness, which can be precisely evaluated only in spatiotemporal context, and our proposed model can be of great use for assessing potential COVID-19 treatment strategies.

Our final synopsis is that the hybrid PDE-ABM model is better suited for thorough and detailed virus spread assessment than the classical ODE system. Following virus propagation on an individual cellular level and taking important spatial effects into account results in a more accurate and complete picture regarding the infection's outcome. Even though the additional integrated details clearly come at a price in terms of computational demand, this pays off very well in the form of information on spatial virus distribution and more accurate predictions.

Stochastic variability

The complex hybrid PDE-ABM approach we considered in chapter allowed us to capture and predict the spatio-temporal viral dynamics in a cell population. Our hybrid model presented two fundamental advantages: firstly, it yielded vital information on the spatial patterns of virus spread, and secondly, its stochastic approach to state changes allowed more realistic simulation outputs. As simulated infection outputs varied based on pure chance, the quantitative assessment of stochastic uncertainty was a crucial remaining task. The present follow-up chapter serves this exact purpose as a supplementary study to chapter : our work successfully tackled non-deterministic variability in a tangible way by elaborating two specific, concrete approaches.

Applying the powerful theory of branching processes we rigorously verified an experimental observation suggested by our previous simulations: once established, infections almost never disappear spontaneously. Specifically, we calculated the probability of spontaneous virus extinction and for a single cell obtained an $\mathcal{O}(0.01)$ value, corresponding to our expectations. We highlight that we successfully estimated the offspring distribution of the branching process describing virus spread: based purely on the original model assumptions and our computer-generated data, we concluded that the number of new infections generated by a single infected cell is best described by a negative binomial distribution – we found a virtually perfect correspondence between the estimated and the observed curves. Our research concerning spontaneous ultimate extinction was conducted for SARS–CoV–2 infections, investigating two different virus removal rates (Figure 4). Increased virus clearance can be viewed as a positive immune response or an effect of treatment, this feature remains to be further investigated as future work.

We completed our study by performing some base-level statistical analysis: we explored fundamental features such as mean and we have calculated a 95% confidence interval for both the number of infected cells and healthy cells (Figure 5). The latter results visually confirmed a reasonable level of variability within our framework: on the one hand, non-deterministic uncertainty allows small and natural changes from outcome to outcome, on

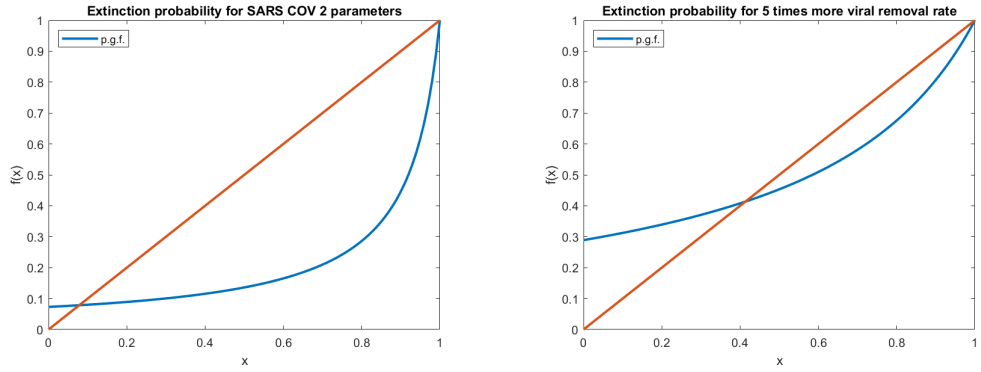

Figure 4: Finding the probability of extinction using the fixed-point method for an experimentally estimated version of the G_X probability generating function. The probability of extinction appears as the intersection of the function G_X with the line $y = x$. **A)** All data were obtained using SARS–CoV–2 parameters. **B)** Data were obtained using a quintupled the virus removal rate compared to SARS–CoV–2 parameters (other parameter values remain unchanged).

the other hand, successful large-scale predictions and analysis remain possible as the vast majority of infection curves remains close to their estimated mean.

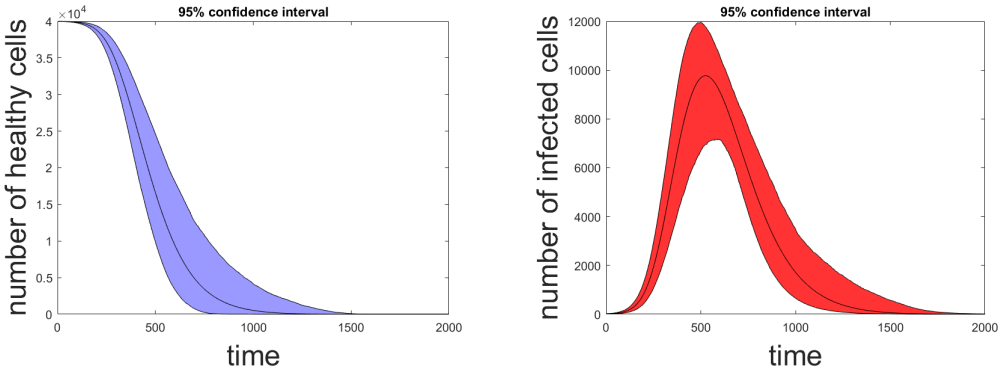

Figure 5: Fundamental statistical features representing stochastic variability for our hybrid PDE-ABM model. Results were obtained by repeatedly running the hybrid simulation 2000 times, always assuming a default SARS–CoV–2 parametrization and $I_0 = 20$. The result shows in a tangible way that while peak sizes vary due to pure chance, the elimination of the cell culture as an outcome is virtually inevitable.

Paxlovid

Even with worldwide vaccination programmes, SARS–CoV–2 and its newly emerging variants represent an unprecedented global challenge. Consequently, new alternative treatment options are still very much needed. This paper yields a mathematical, computation-based evaluation of one of the most promising SARS–CoV–2 inhibitors to date, Paxlovid. We implemented and carefully calibrated a multiscale mathematical framework (Equation (8)) to serve as a

small *in silico* laboratory where the basic features of Paxlovid can be replicated, explained, and further investigated.

$$\begin{cases} \frac{\partial V(t,x,y)}{\partial t} = D_V \Delta V - \mu_V V + (1 - \eta_N(N)) \cdot \sum\limits_{(i,j)\in\mathcal{J}} g_{i,j}(t,x,y), t > 0, \ (x,y) \in \Omega, \\ \\ \frac{\partial V(t,x,y)}{\partial \nu} = 0, \quad t > 0, \ (x,y) \in \partial\Omega, \end{cases} \tag{8}$$

Our calculations correspond to clinical expectations remarkably well: we successfully replicated the outcome of a real-life *in vitro* experiment in the simulated context of our model (Figure 6), moreover, both the sufficiency and the necessity of Paxlovid's two main components were verified by our computations for a simplified *in vivo* case.

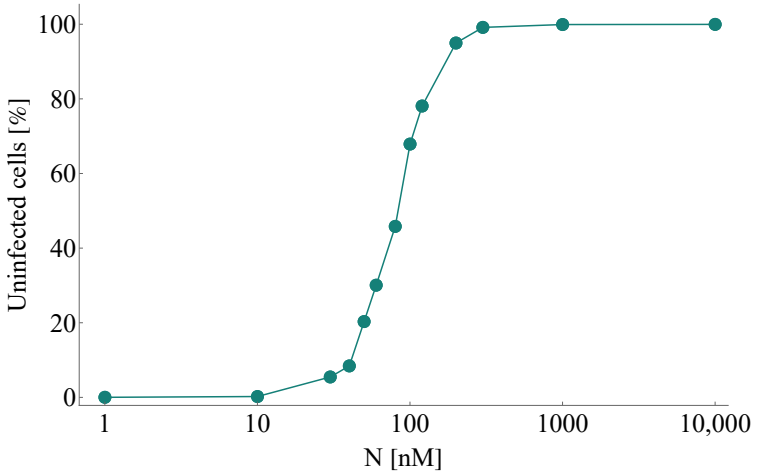

Figure 6: A simulated series of *in vitro* experiments with increasing initial nirmatrelvir concentrations. Concentration levels are assumed to be constant throughout the entire course of each experiment. Every simulation follows the emerging infection dynamics for 4 days. SARS–CoV–2 infection and nirmatrelvir treatment are initialized simultaneously. Our computer-generated predictions correspond reassuringly to real-life scientific measurements assessing infection inhibition of PF-07321332, see Figure 3D in [9].

To further improve Paxlovid's assessment, we generated a heatmap investigating the results' sensitivity to the inherently vaguely specified virus diffusion coefficient.

The proposed hybrid model has its limitations. In its present form, the system operates on a simplistic two-dimensional grid, ignoring the complex 3D geometry of the lungs, which may introduce bias or delays in the predictions. The implementation of a biologically more realistic three-dimensional structure falls beyond the scope of this study and is subject of future research. The increase of dimension (and of lattice size) inevitably affects the computational load and, hence, requires additional, technical optimization of the code in order to achieve the desired performance. Similarly, the current assumption of a constant virus clearance rate is ignoring the intricacies of the immune system that is a major limitation when considering *in vivo* scenarios. While in real life there is a significant virus release at burst, our model is averaging out the virus source over a time interval, hence we work with

constant virus production rates, similarly to [6] and [7]. Consequently, this limitation is responsible for a slight overestimation regarding advancement of virus release. We note that in the context of our model it is straightforward to implement more sophisticated approaches as well (which would not be the case for example in an ODE-based system), and we also highlight that our source code includes a built-in option allowing to consider latency periods. However, that would require sufficiently detailed biological data for parametrization. Finally, we mention that our basic modeling approach to natural cellular life cycles, though being a simplification, is not expected to imply significant deviation from reality in the context of a 5-day long Paxlovid treatment: natural cell death is responsible only for circa 1% of cell population loss during this time frame according to the 17-month half-life of epithelial lung cells [8].

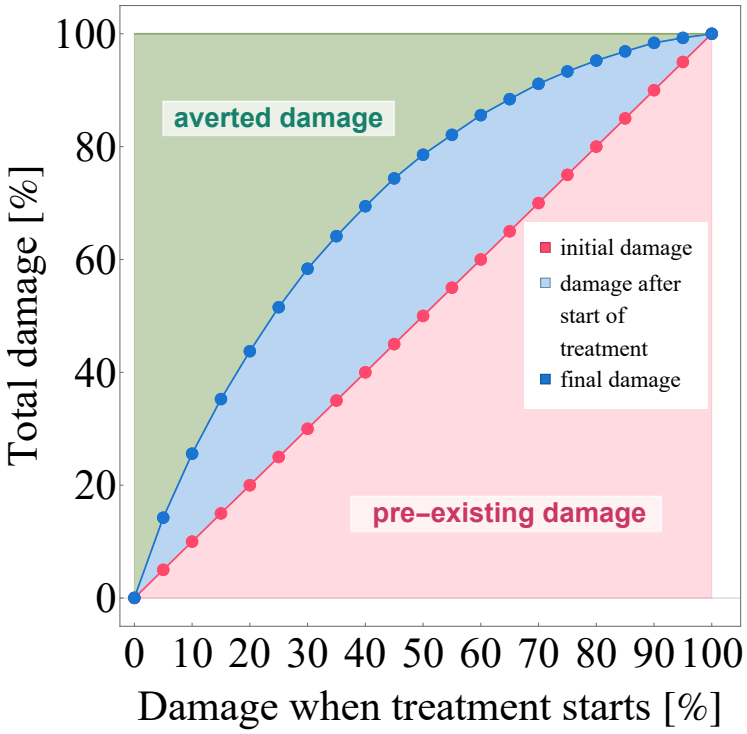

Figure 7: The visualization of averted damage as a result of Paxlovid treatment. The quantity on the horizontal axis (and the $x = y$ line itself) represents the level of cell culture damage suffered until Paxlovid treatment begins, while data points depicted in blue show the unavoidable further damage that occurs after therapy commences. The shaded areas are a precise visual representation of *initial damage* (red), *unavoidable post-intervention damage* (blue), and *averted damage* (green). Evidently, the light green area represents those healthily functioning epithelial lung cells that were ultimately saved by Paxlovid.

Despite the mathematical model's necessary simplifications and the short scope of this case study we were able to visualize and verify the importance of early interventions (see Figure 7), moreover, we highlight that such hybrid models and computational frameworks hold a great deal of promise with applications such as supporting clinical trials by means of *in silico* experiments. Computation-based evaluation and simulation of therapies not only

can enhance optimization of treatments, but a further development of this technology could also serve to reduce the need for animal testing in the future.

Bibliography

[1] Macal CM, North MJ. Tutorial on agent-based modeling and simulation. In Proceedings of the Winter Simulation Conference, 2005. 2005 Dec 4 (pp. 14-pp). IEEE.

[2] Arduin H, de Cellès MD, Guillemot D, Watier L, Opatowski L. An agent-based model simulation of influenza interactions at the host level: insight into the influenza-related burden of pneumococcal infections. BMC infectious diseases. 2017 Dec;17(1):1-2.

[3] Bravo RR, Baratchart E, West J, Schenck RO, Miller AK, Gallaher J, Gatenbee CD, Basanta D, Robertson-Tessi M, Anderson AR. Hybrid Automata Library: A flexible platform for hybrid modeling with real-time visualization. PLoS computational biology. 2020 Mar 10;16(3):e1007635.

[4] Baccam P, Beauchemin C, Macken CA, Hayden FG, Perelson AS. Kinetics of influenza A virus infection in humans. Journal of virology. 2006 Aug 1;80(15):7590-9.

[5] Bocharov GA, Romanyukha AA. Mathematical model of antiviral immune response III. Influenza A virus infection. Journal of Theoretical Biology. 1994 Apr 21;167(4):323-60.

[6] Lord, J.S.; Bonsall, M.B. The evolutionary dynamics of viruses: virion release strategies, time delays and fitness minima. *Virus Evol* **2021 Apr 27**;*7(1)*:veab039.

[7] Perelson, A.S. Modelling viral and immune system dynamics. *Nat Rev Immunol* **2002 Jan**;*2(1)*:28–36.

[8] Rawlins, E.L.; Hogan, B.L.M. Ciliated epithelial cell lifespan in the mouse trachea and lung. *Am J Physiol Lung Cell Mol Physiol* **2008 Jul**;*295(1)*:L231–4.

[9] Owen, D.R.; Allerton, C.M.; Anderson, A.S.; Aschenbrenner, L.; Avery, M.; Berritt, S.; Boras, B.; Cardin, R.D.; Carlo, A.; Coffman, K.J.; Dantonio, A.; et al. An oral SARS-CoV-2 Mpro inhibitor clinical candidate for the treatment of COVID-19. *Science* **2021 Dec 24**;*374(6575)*:1586–93.

[10] Outlaw VK, Bovier FT, Mears MC, Cajimat MN, Zhu Y, Lin MJ, Addetia A, Lieberman NA, Peddu V, Xie X, Shi PY. Inhibition of coronavirus entry in vitro and ex vivo by a lipid-conjugated peptide derived from the SARS-CoV-2 spike glycoprotein HRC domain. MBio. 2020 Sep 1;11(5):e01935-20.